

Article

# A Study on Welding Deformation in Fiber Laser Welding of 9% Nickel Steel through Finite Element Analysis Part I: Implementation of Welding Heat Source Model

Changmin Pyo <sup>1</sup>, Jaewoong Kim <sup>1</sup> and Du-Song Kim <sup>2,\*</sup>

<sup>1</sup> Smart Manufacturing Process R&D Group, Korea Institute of Industrial Technology, Gwangju 61012, Korea; changmin@kitech.re.kr (C.P.); kjw0607@kitech.re.kr (J.K.)

<sup>2</sup> Welding Engineering R&D Department, Daewoo Shipbuilding Marine Engineering, Geoje 53302, Korea

\* Correspondence: dusong@dsme.co.kr

**Abstract:** Due to various environmental regulations, the demand for natural gas, i.e., a clean energy, is expected to increase continuously. In terms of efficient storage and transportation of natural gas, liquefied natural gas has an advantageous volume of 1/600 compared to natural gas, but the materials that can be used at a cryogenic temperature of  $-163\text{ }^{\circ}\text{C}$  are limited. A 9% nickel steel is a material recommended by IMO through IGC. It has excellent mechanical properties compared to other cryogenic materials, but its use has been limited due to its disadvantages in arc welding. Therefore, the main topic of this study is the automatic welding of 9% nickel steel using fiber laser and its purpose is to predict the welding deformation during fiber laser welding. First, an investigation was conducted to find the fiber laser welding heat source. A model that can cover all the models in prior studies such as curve, exponential, conical, conical-conical combination, and conical-cylinder combination models was proposed and the heat source model was constructed in a multi-layer format. Heat transfer analysis was performed using the ratio of a heat source radius and heat energy of each layer as a variable and the pass or failure of a heat source was determined by comparing the analysis results to the experimental results. By changing the variables in conjunction with the optimization algorithm, the main parameters of a passed heat source model were verified in a short period of time. In addition, the tendency of parameters according to the welding speed was checked.

**Keywords:** fiber laser welding; 9% nickel steel; welding heat source model; FEM; global optimization



**Citation:** Pyo, C.; Kim, J.; Kim, D.-S. A Study on Welding Deformation in Fiber Laser Welding of 9% Nickel Steel through Finite Element Analysis Part I: Implementation of Welding Heat Source Model. *Processes* **2021**, *9*, 2188. <https://doi.org/10.3390/pr9122188>

Academic Editor: Kody Powell

Received: 2 November 2021

Accepted: 2 December 2021

Published: 4 December 2021

**Publisher's Note:** MDPI stays neutral with regard to jurisdictional claims in published maps and institutional affiliations.



**Copyright:** © 2021 by the authors. Licensee MDPI, Basel, Switzerland. This article is an open access article distributed under the terms and conditions of the Creative Commons Attribution (CC BY) license (<https://creativecommons.org/licenses/by/4.0/>).

## 1. Introduction

Due to global warming and environmental pollution, regulations on fossil fuels are becoming stricter. For ships, SO<sub>x</sub> and NO<sub>x</sub> emitted from a diesel engine are the main targets of regulation and regulations forced ships to be installed a scrubber on diesel engines for desulfurizing purposes. However, in order to devise a more permanent and fundamental solution, increased research and field application in the industrial field on how to use liquefied natural gas (LNG) as a fuel are being pursued [1,2].

Liquefied natural gas is not subject to environmental regulations because it does not emit SO<sub>x</sub> or NO<sub>x</sub> during combustion. However, its boiling point is  $-163\text{ }^{\circ}\text{C}$ , so special care is required during handling. Most materials containing a metal cannot perform their role properly because low-temperature brittleness occurs when exposed to cryogenic temperatures. The International Marine Organization (IMO) specifies the materials that can be used at the LNG boiling point in the IGC Code, and these materials are STS304L, STS316L, Invar (36% nickel steel), high manganese steel, and 9% nickel steel [3]. Among these metals, 9% nickel steel is one of the more popular materials due to its excellent mechanical properties such as yield strength and tensile strength at  $-163\text{ }^{\circ}\text{C}$ . Also toughness is higher than mild steel, especially in a cryogenic condition, it can be used for LNG carriers [3].

A process required to make a product using the above material is welding, which is the most common process in the industrial field due to its relatively low operating cost and easy access. Arc welding has been typically used and there have been studies using manual welding such as FCAW (flux core arc welding) for 9% nickel steel. Na compared the welding quality when 9% nickel steel was welded by GTAW or FCAW [4] and Kim studied the design of an LNG fueled ship using 9% nickel steel [5]. Yun studied the optimal welding method for the fillet welding of 9% nickel steel [6].

However, 9% nickel steel had a limitation with regard to its wide application despite its excellent material properties because of arc deflection due to magnetization during manual welding of FCAW and its filler metal is 10~25 times more expensive than other cryogenic materials [7–9]. Therefore, this study attempted to solve the above problem by studying automatic welding that employs fiber laser welding that does not use a filler metal. Fiber laser gives a concentrated heat source to a narrow area for a short period of time to minimize thermoelastic deformation and its high welding speed enables increased productivity [10].

There have been studies on the welding of 9% nickel steel by applying fiber laser welding. Huang conducted a study where a filler metal was used for fiber laser welding of 9% nickel steel [9] and Choi conducted a study on 9% nickel steel as a material for type B LNG fuel tank [11]. Park performed and analyzed super TIG welding to weld 9% nickel steel [12].

The main purpose of this study was to predict the amount of welding deformation and deformation patterns through finite element analysis when welding 9% nickel steel, i.e., a cryogenic material, using a fiber laser. In particular, the main goal of this study was to find a high-quality welding heat source, and the welding heat source was assumed to be a model composed of five layers. This is similar to the method in a prior study where a welding heat source was discovered during fiber laser welding of STS304L [13–15]. It is a model where the heat source radius and the ratio of heat source per layer are different for each layer of the heat source.

Goldak's double ellipse model [16,17], which is the most widely used in typical arc welding, has the disadvantage that it cannot simulate the keyhole shape that occurs during laser welding [18,19], so various models have been proposed.

Kim proposed a model of a circular cone shape as a welding heat source, performed finite element analysis, predicted a fusion zone, and verified it through an experiment [20]. Farrokhi used a model where a conical shape and the Gaussian distribution were combined and verified it through finite element analysis and an experiment [21]. Xu implemented and verified a heat source shape that connects the upper and lower circular surfaces in a quadratic fashion in a conical shape and the details are shown in Figure 1a [22]. As a heat source model, Evdokimov implemented and verified a heat source shape that exponentially connects the top and bottom circular surfaces in a conical shape and the details are shown in Figure 1b [23]. Kik performed verification using a combination of two conical shapes and also a combination of a conical shape and a cylinder shape as a heat source model and the details are shown in Figure 1c [24].

A common characteristic of prior studies is that a heat source was estimated based on the shape of a weld bead and it was used as the heat source for a finite element analysis model. It has been confirmed that a simple conical-conical shape develops into an exponential model, a conical-conical or conical-cylinder combination, which is due to the fact that it is difficult to find a heat source for laser welding just by using a simple model. Actually many researches [25–35] related to a laser welding heat source model have their own model. In addition, the determination of the main dimension to determine a heat source shape in the above studies is based on the welding experiment results and the fusion zone dimension of a SEM photograph, so there is a limitation in that it is difficult to implement the formula of a general welding heat source according to welding conditions.

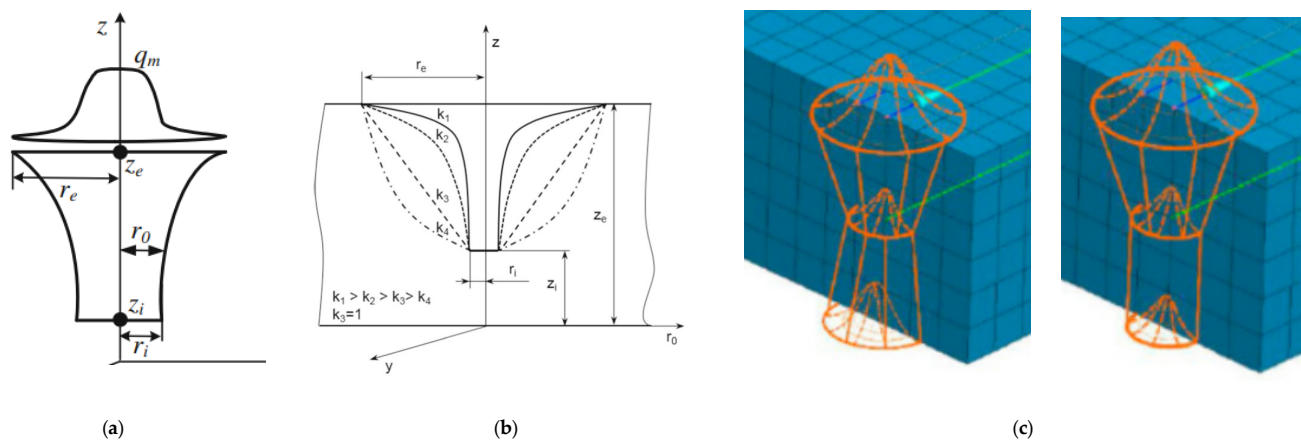


**Figure 1.** Laser heat source models. (a) Curve model; (b) exponential model; (c) conical-conical and conical-cylindrical models.

As the first step to derive the general welding heat source equation, the purpose of this study was to derive the shape of a welding heat source using a welding heat source model with a high degree of freedom. By dividing the heat source into five layers, a model that varies the welding heat source radius and the heat source ratio for each layer was developed and the fusion zone was estimated using finite element analysis. Then, after the experiment, the heat source radius and the ratio of heat source for each layer were found compared to the fusion zone in the SEM picture. Then, an optimal heat source model was sought by linking the global optimization algorithm and finite element analysis.

## 2. Simulation Using Experimental and Finite Element Analysis Models

### 2.1. Welding Test Equipment and Test Conditions

For this study, a fiber laser welding machine with a capacity of 5 kW was used. Miyachi welding equipment was used and it consists of a laser welding oscillator, optical system, controller, and chiller, as shown in Figure 2. The spot diameter of the optical system was 400  $\mu\text{m}$ , its focal length was 148.8 mm, the focal depth was 6 mm, the defocus was set to 0, and  $\text{N}_2$  was used as a protective gas and sprayed at a rate of 15 L/min. Both tilting and working angle were fixed at  $0^\circ$ . During the experiment, the power was fixed at 4 kW and the experiment was performed while changing the speed to 1.5 m/min, and 2.0 m/min.



**Figure 2.** Fiber laser welding system.

## 2.2. Weld Bead Analysis

The size of a welding specimen was 600 mm × 300 mm × 6 mm and the center part was cut to 10 mm in the welding direction and 25 mm in the width direction and its cross-sectional observation was performed. Polishing was performed to clearly check the shape of a bead and etching was performed using a nital solution (10% HNO<sub>3</sub>, Ethanol).

As shown in Figure 3, a digital optical microscope with a resolution of 2 mega pixels was used to measure the welding deformation. The shape of a fusion part caused by welding was classified according to top bead width and penetration and its size was checked for bead shape simulation. The shape and size information of a bead is shown in Figure 4.

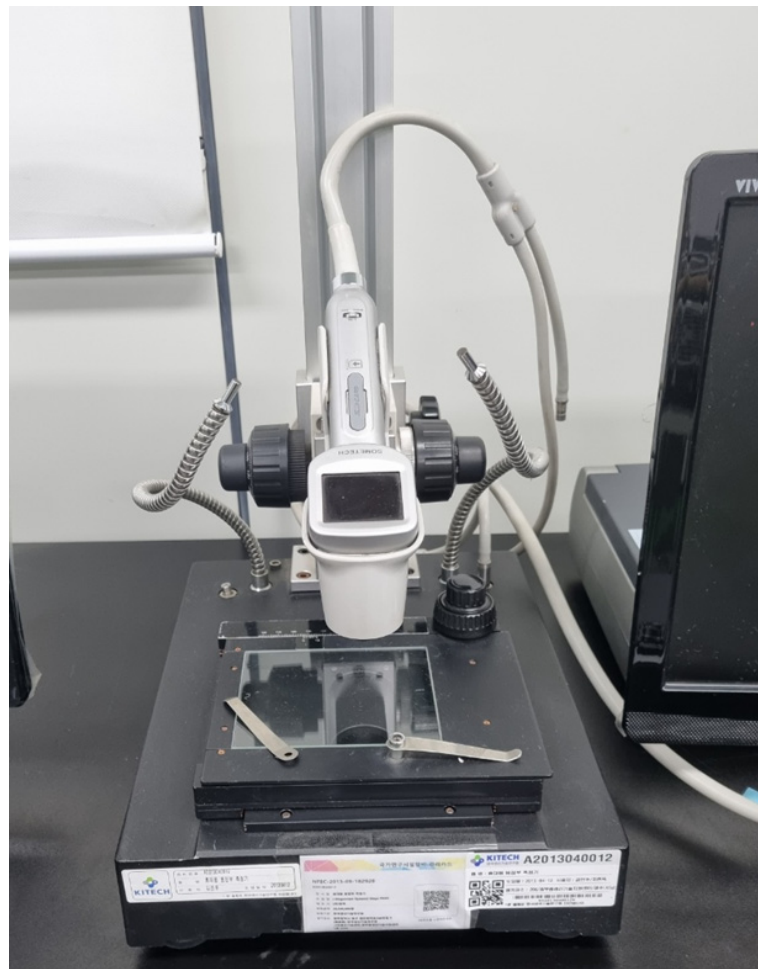
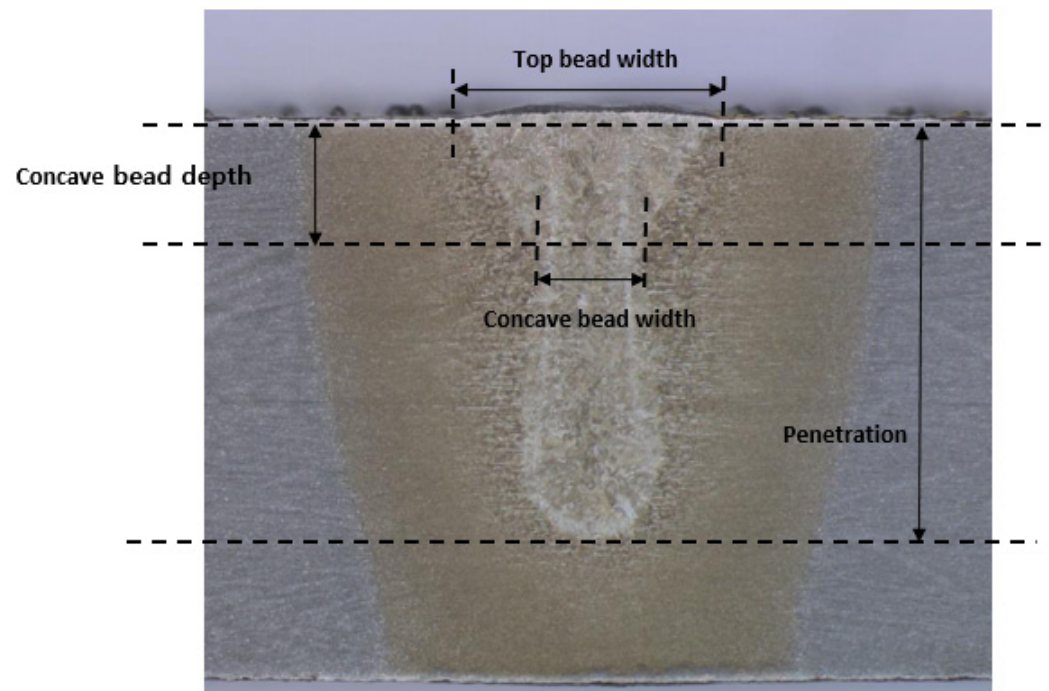


Figure 3. Optical microscope equipment.



**Figure 4.** Welding bead shape and dimension.

### 2.3. Finite Element Analysis Software

In this study, the optimization algorithm and finite element analysis were used together and Abaqus2020 and Isight2020 from Dassault System were employed. In addition, the user subroutine technique using Fortran was utilized to simulate the moving heat source. The implementation of a welding heat source using Abaqus and Fortran has been adopted in many prior studies [36–38] and the optimal design using Isight has also been used in many prior studies [39,40].

### 2.4. Material Properties by Temperature

Table 1 [41] shows the chemical composition of 9% nickel steel used in this study.

**Table 1.** Chemical composition of 9% nickel steel (wt%).

Material	C	Si	Mn	S	P	Ni	Fe
A553-1	0.05	0.67	0.004	0.003	0.25	9.02	Bal.

For the heat transfer analysis using finite element analysis, material properties such as specific heat, thermal conductivity, and density are required. Although deriving material properties through measurement is the most accurate method, there is a limitation in deriving material properties near the melting point. In a prior study, properties by temperature were derived using JMatpro [42] and material properties were derived using JMatpro in this study too. The details are shown in Figure 5.

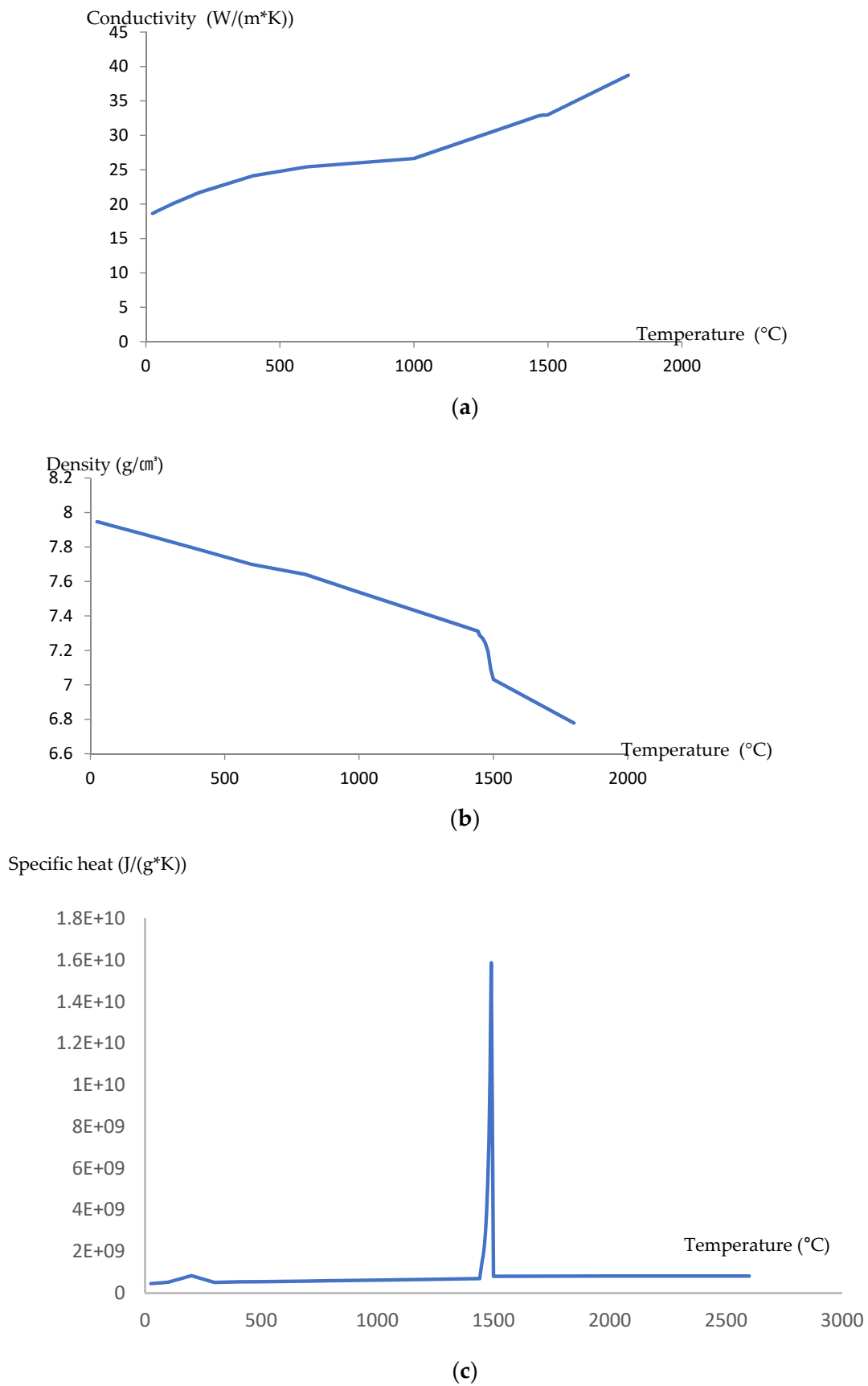


Figure 5. Material properties of 9% nickel steel by temperature. (a) Conductivity; (b) density; (c) specific heat.

### 2.5. Welding Heat Source Model

The welding heat source model is configured as an integrated heat source model that can cover all existing laser heat source models. Existing heat source models are constructed based on a conical model which is based on a Gaussian distribution heat source. In this study, a cone-based model consisting of multiple layers was adopted. By selecting a different heat source radius for each layer, it was possible to cover all of the existing heat source models such as the conical model (typical heat source model), the secondary interpolation conical model, the exponential interpolation conical model, the conical-cylindrical combination model, and the conical-conical model. The shape of a heat source model is shown in Figure 6. The distribution of a heat source for each layer was defined to follow a Gaussian distribution as in typical heat source models.

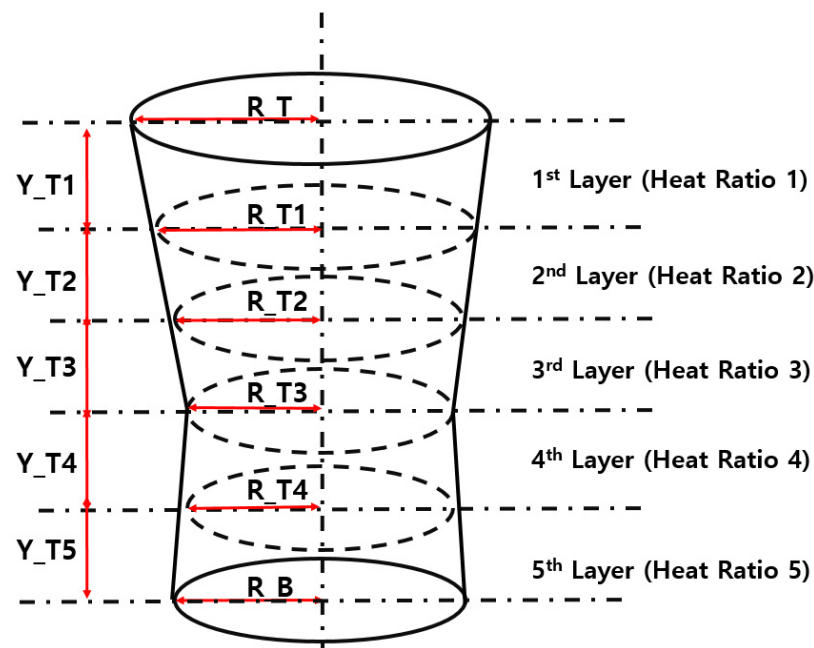


Figure 6. Multi-layered laser welding heat source model.

The height of all layers was set to be the same and the radius of each layer and the thermal energy ratio of each layer was set as the main variable. In addition, a total of 12 variables was set by configuring the welding efficiency and the height of a welding heat source as variables. The heat source distribution in each layer follows a Gaussian distribution and the equation is as follows. The heat source distribution of each layer is shown in Equations (1) and (2) and the meaning of the variables in Equation (1) is shown in Table 2.

$$q(x, y, z) = \frac{9Qe^3}{\pi(e^3 - 1)(Y_{T1})(R_T^2 + R_T R_{T1} + R_{T1}^2)} \exp\left(\frac{3[(x - vt)^2 + z^2]}{(R_1(y))^2}\right) \quad (1)$$

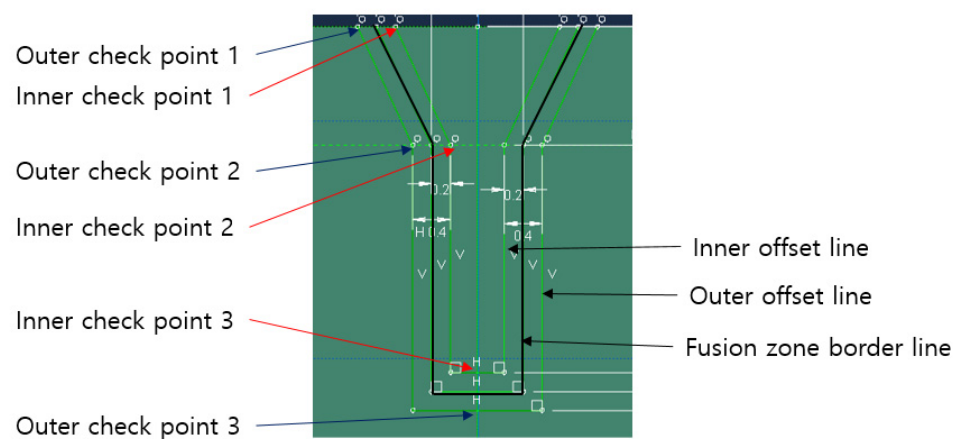
$$R_1(y) = R_T - (R_T - R_{T1}) \frac{y_T - y}{y_T - y_{T1}} \quad (2)$$

**Table 2.** Variables of heat source model.

Variables	Meaning
Efficiency	Welding efficiency
$R_T$	Top radius of 1st layer (top layer)
$R_{T1}$	Top radius of 2nd layer
$R_{T2}$	Top radius of 3rd layer
$R_{T3}$	Top radius of 4th layer
$R_{T4}$	Top radius of 5th layer
$R_B$	Bottom radius of 5th layer
Heat Ratio 1	Heat ratio of 1st layer
Heat Ratio 2	Heat ratio of 2nd layer
Heat Ratio 3	Heat ratio of 3rd layer
Heat Ratio 4	Heat ratio of 4th layer
Heat Ratio 5	Heat ratio of 5th layer
Heat depth	Length of heat source in depth direction

### 2.6. Research Process

Finite element analysis was performed while changing the variables of the welding heat source model introduced in Section 2.5 and the coefficients of the welding heat source model suitable for each welding condition were sought through a parametric study that compares the analysis results with actual experimental results. For the comparison with actual experimental results, the shape of a bead was reflected in the finite element analysis modeling and the shape offset by 0.2 mm from the bead was reflected in the modeling. The inner side of a bead must exceed the melting point of 9% nickel steel at least once during the welding process and the outer side must not exceed the melting point even for a moment. As shown in Figure 7, the suitability of heat source parameters was judged by setting three points each in the internal/external offset shape.

**Figure 7.** Fusion zone border line and temperature check points.

### 2.7. Boundary Conditions of Heat Transfer Analysis

To perform the parametric study introduced in Section 2.6, a heat source was searched for by performing heat transfer analysis for 1000~2000 models for each welding condition. Therefore, an analysis model was constructed that minimizes the number of grids although modeling was basically performed under similar conditions to the experiment. In particular, the analysis was performed by reducing the length in the welding direction and its validity was verified in previous similar studies [36]. The model is shown in Figure 8.

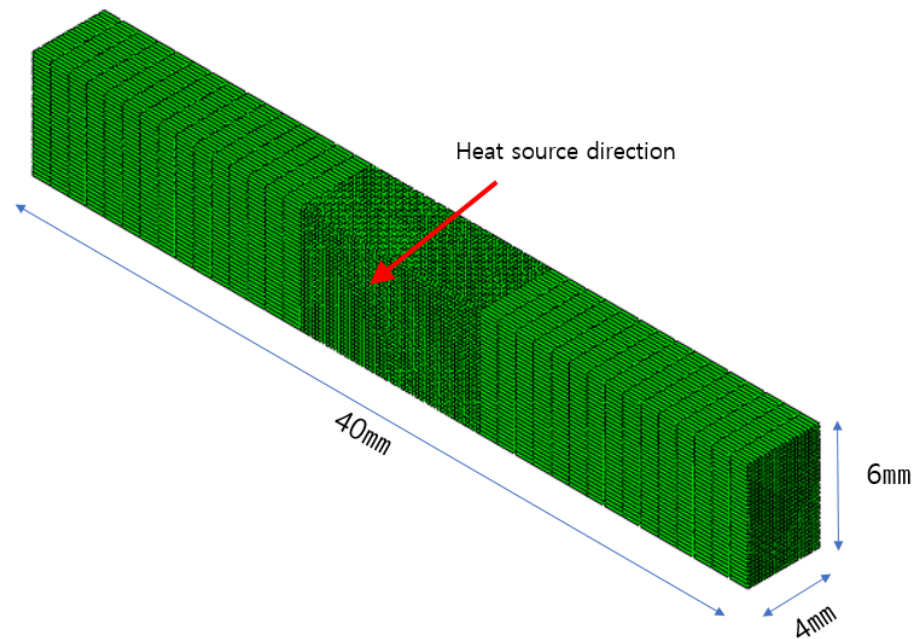


**Figure 8.** Simplified model.

Welding speed and welding power were performed under the same conditions as the actual experiment and an analysis considering both convective heat transfer and radiative heat transfer was performed. The convective heat transfer coefficient was set to  $20 \text{ W/m}^2\text{K}$ , the emissivity was set to 0.8, and the atmospheric temperature was set to  $20 \text{ }^\circ\text{C}$ . Those conditions are referred to other research [43,44].

### 2.8. Optimization Algorithm

For this study, adaptive simulated annealing (ASA), one of the global optimization techniques, was used as an optimization algorithm. ASA is one of the probabilistic methodologies to find an optimal value in the global search space and it was inspired by the annealing process that seeks to reduce metal defects. It is a process of deriving an optimal value by searching for an optimal value by increasing the change of variables, not falling into a local optima, and reducing the variable change while conducting a case study. The advantage of ASA is that it reduces the time taken for optimization by automatically adjusting the variable change range according to the optimization trend [45].

ASA has already been used for design optimization in the electronics and bio industries, and has also been applied to welding research [46].

## 3. Results

### 3.1. Welding Test Results

As mentioned in Section 2, welding was performed by using a fiber laser at different welding speeds while the welding power was fixed. Experiments were conducted in two speeds, i.e.,  $1.5 \text{ m/min}$  and  $2.0 \text{ m/min}$  and cross-sectional observation was performed. The cross-sectional observation results are shown in Figure 9.

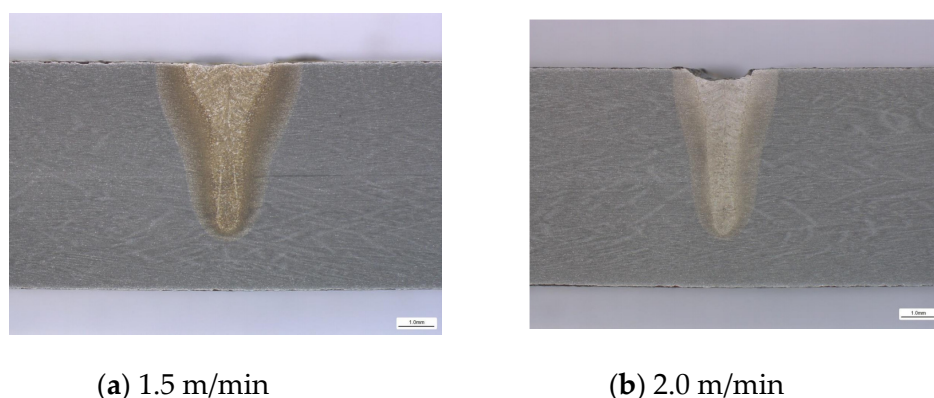


**Figure 9.** Cross-sectional observation results.

As mentioned in Section 2.2, the penetration shape was classified according to four major dimensions: top bead width, concave bead width, concave bead depth, and penetration. The data are shown in Table 3.

**Table 3.** Key bead dimension per welding speed.

Welding Speed (m/min)	Top Bead Width (mm)	Concave Bead Width (mm)	Concave Bead Depth (mm)	Penetration (mm)
1.5	2.583	1.075	2.275	4.867
2.0	1.717	0.941	1.410	4.860

### 3.2. Results of Welding Heat Source Model Search

The 11 parameters of the welding heat source model introduced in Section 2 were checked based on the key welding bead dimensions introduced in Section 3.1 and the results are shown in Table 4.

**Table 4.** Key parameters of welding heat source per welding speed.

	1.5 Mpm	2.0 Mpm
EFFICIENCY	0.884	0.873
R_T	2.164	2.110
R_T1	0.446	1.454
R_T2	0.357	1.075
R_T3	0.781	0.371
R_T4	0.861	0.869
R_B	4.010	1.184
HEAT_depth	5.242	4.885
Heat Ratio 1	0.233	0.292
Heat Ratio 2	0.327	0.124
Heat Ratio 3	0.018	0.203
Heat Ratio 4	0.148	0.189
Heat Ratio 5	0.274	0.192

In addition, it was found that the shape of a welding heat source is the shape of a conical-conical combination under all three conditions as shown in Figure 10.

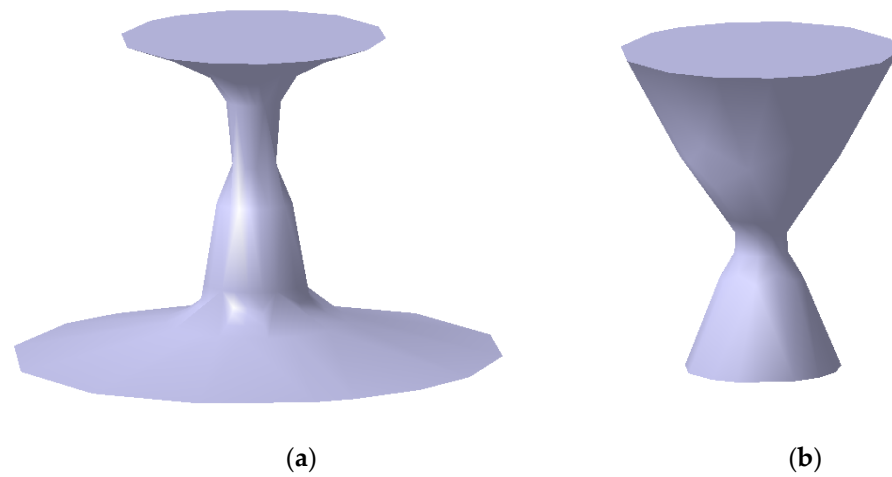


**Figure 10.** The shape of a heat source per welding speed. (a) 1.5 m/min; (b) 2.0 m/min.

In addition, the results of heat transfer analysis using three different heat sources are shown in Figures 11 and 12 and it was found that they are similar to the fusion zone line of cross-sectional observation results in Figure 10.

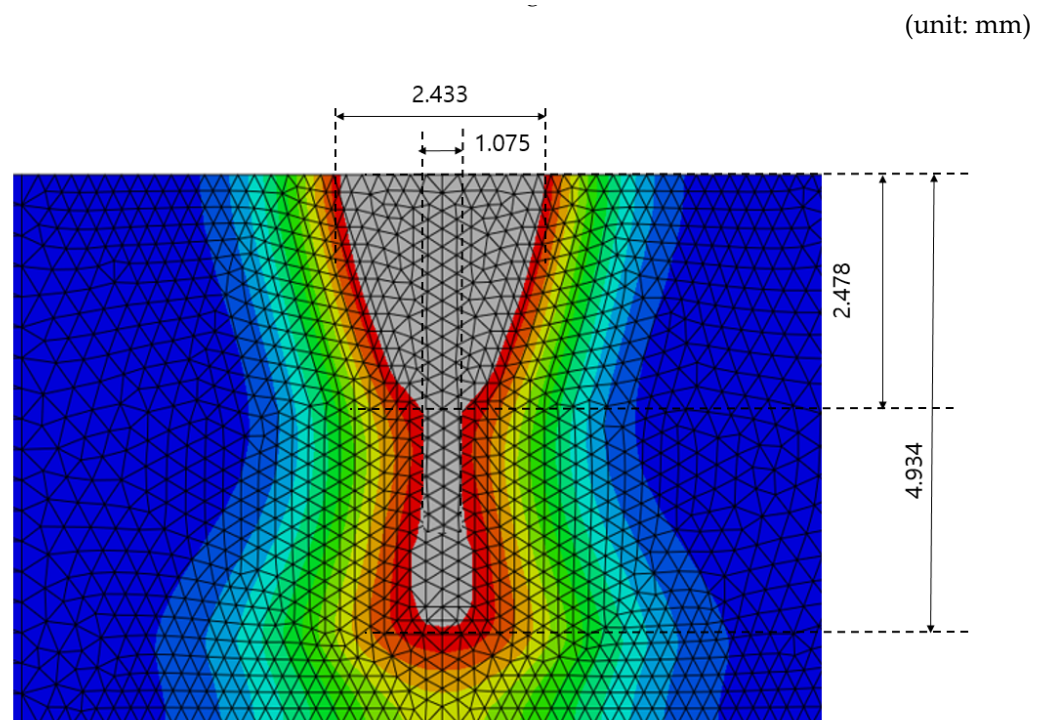


**Figure 11.** Heat transfer analysis results per welding speed (1.5 m/min).

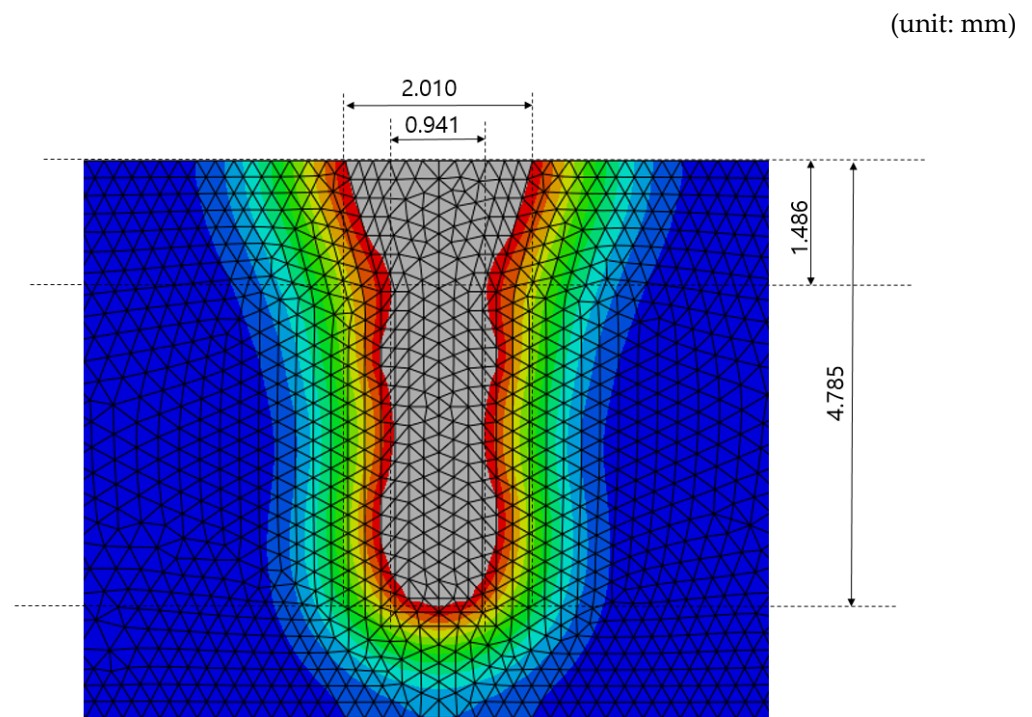


**Figure 12.** Heat transfer analysis results per welding speed (2.0 m/min).

#### 4. Discussion

As shown in Table 4, it was found that the energy efficiency is similar for all two cases. When the fiber laser welding was performed on 9% nickel steel, it was found that the welding efficiency was about 87~88% and the welding efficiency was very high compared to arc welding.

As the welding speed increases, the amount of energy input per hour is reduced and it is expected that the size of a welding heat source will be affected. The depth of a welding heat source (heat depth) follows the trend as shown in Figure 13.

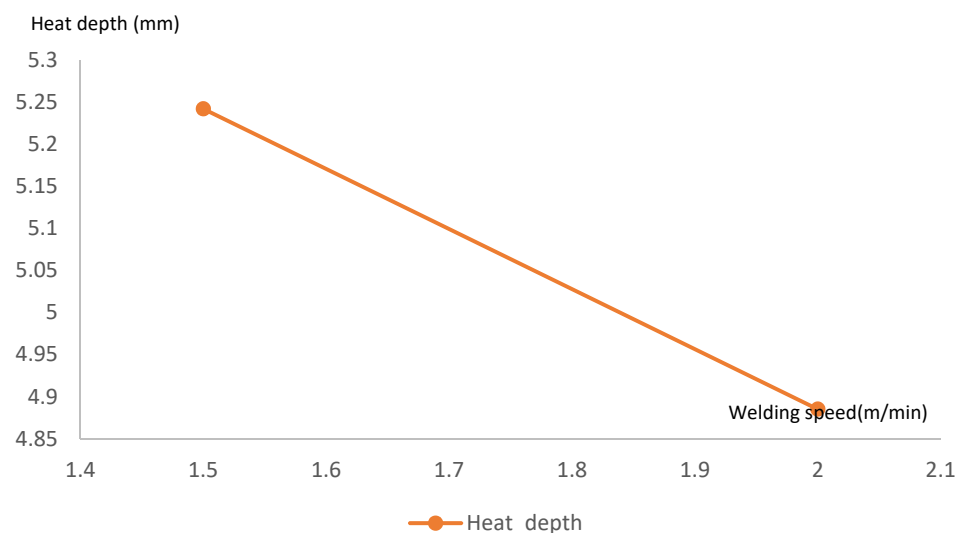


**Figure 13.** Heat depth tendency per welding speed.

For the shape of a welding heat source, it was found that all two cases showed a shape close to the conical-conical one. In particular, it was found that the Radius ( $R_B$ ) of a heat source in Layer 5 increased to 60% or more compared to the Radius ( $R_T$ ) of a heat source in the top layer and the smallest Radius appeared in Layer 3 under all conditions.

In this study, it was assumed that the ratio of heat source energy per layer was different. In prior studies, it was assumed that the energy ratio of two layers is the same when they are divided into two layers [21]. The latter case has a limitation in that the energy density becomes higher at the lower layer where the radius becomes smaller. In a prior laser welding heat source-related study, the heat source is defined as a primary heat source if the laser heat source is irradiated to the top of a base material and the heat source is defined as a secondary heat source when the heat source turns into a plasma state and creates a keyhole due to flow [21–24]. It is not realistic to assume the same energy ratio for each layer, so a parametric study was performed in this study by assuming that the energy ratio for each layer was also an independent variable. Therefore, as shown in Figure 14, it was found that the sum of energy ratios in Layer 1 and Layer 2 was 61% at 1.5 mpm, and 42% at 2.0 mpm. As a result, it can be inferred that the concentration of heat energy at the top part of a heat source is higher when the speed is lower. In this experiment, it was found that the concentration of energy by height appeared evenly when the speed was 2.0 mpm (Figure 15).

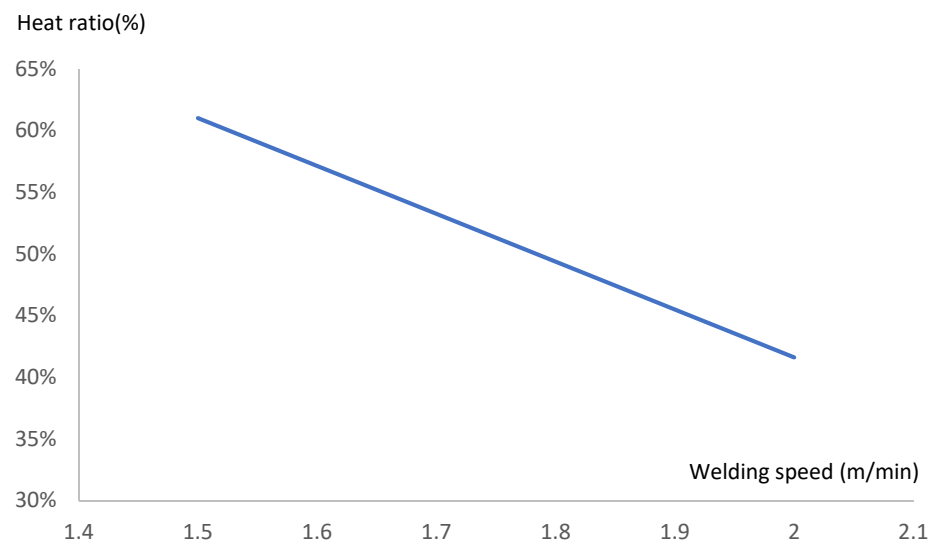


Figure 14. Energy ratio of top 2 layers per welding speed.

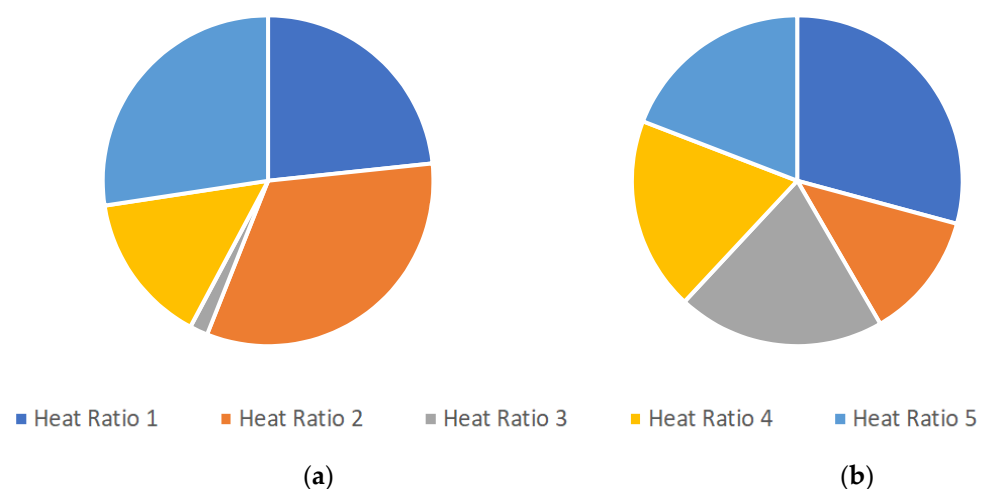


Figure 15. Energy concentration by layer per welding speed. (a) 1.5 m/min; (b) 2.0 m/min

The main purpose of this study was to implement an integrated heat source model, to find the key parameters of a heat source per welding condition, and to check the trend of parameters according to the welding speed, which is the key welding condition. There is a limitation, however, because there are only two cases compared and the welding test

also has a limitation in that in order to ensure the reliability, the experiments should be repeated more than five times. Nevertheless, this study is meaningful in that it attempted to implement an integrated heat source model that has never existed before. In future research, it is planned to conduct a study that precisely analyzes the trend of parameters for each welding condition by further defining more welding speeds and conducting a study that compares not only the welding speed but also the welding power.

## 5. Conclusions

This study is an initial research effort to implement a general model regarding a fiber laser welding heat source. The constructed heat source model in a multi-layer form can cover all the models including curve, exponential, conical, conical-conical combination, conical-cylindrical combination that have featured in prior studies.

1. The temperature distribution was checked through the heat transfer analysis using a moving heat source by simulating the fiber laser welding experiment of STS304L.
2. Heat transfer analysis was performed using the heat source radius and the ratio of heat energy for each layer as variables and the pass or failure of a heat source was determined by comparing it to the experimental results. By changing the variables in conjunction with the optimization algorithm, a heat source model with pass condition was found in a short period of time.
3. Each analysis was performed with different welding speeds and it was found that the welding heat source at 1.5 m/min, and 2.0 m/min under 4 kw condition was similar to the conical-conical combination model.
4. From the analysis according to the welding speed, it is found that welding speed and the heat depth are inversely related. In addition, the energy ratio was different for each layer of a heat source and the concentration of the upper part of a heat source was higher as the speed is lower.
5. In future research, the relationship between the welding conditions and the heat source model will be checked by comparing the heat source model under the welding conditions with different welding power and welding speed, and ultimately, a study will be performed to find a general heat source model for fiber laser welding.

**Author Contributions:** Conceptualization, C.P. and D.-S.K.; methodology, C.P.; software, C.P.; validation, J.K.; formal analysis, J.K.; investigation, C.P.; writing—original draft preparation, C.P.; writing—review and editing, D.-S.K.; visualization, C.P.; supervision, J.K.; project administration, J.K.; funding acquisition, J.K. All authors have read and agreed to the published version of the manuscript.

**Funding:** This study was conducted with the support of the Korea Institute of Industrial Technology as “The dynamic parameter control based smart welding system module development for the complete joint penetration weld (KITECH EH-21-0003)”.

**Institutional Review Board Statement:** Not applicable.

**Informed Consent Statement:** Not applicable.

**Data Availability Statement:** The data presented in this study are available on request from the corresponding author.

**Conflicts of Interest:** The authors declare no conflict of interest.

## References

1. Kim, J.; Kim, J. The Characteristics of Continuous Waveshape Control for the Suppression of Defects in the Fiber Laser Welding of Pure Titanium Sheet (I). *J. Weld. Join.* **2016**, *36*, 62–68.
2. Kim, J.; Kim, J.; Pyo, C. A Study on Fiber Laser Welding of High-Manganese Steel for Cryogenic Tanks. *Processes* **2020**, *8*, 1536. [[CrossRef](#)]
3. Kim, D.S.; Pyo, C.; Kim, J.; Kim, J.; Lee, H.K. A Study on Cross-Shaped Structure of Invar Material Using Cold Wire Laser Fillet Welding (PART I: Feasibility Study for Weldability). *Metals* **2020**, *10*, 1385. [[CrossRef](#)]
4. Na, K.; Lee, C.; Park, J.; Cho, M. A Comparison of Hot Cracking in GTAW and FCAW by Applying Alloy 625 Filler Materials of 9% Ni Steel. *J. Weld. Join.* **2019**, *37*, 357–362. [[CrossRef](#)]

5. Kim, B.; Park, J.; Lee, J.; Kim, M. Study on the Initial Design of an LNG Fuel Tank using 9 wt.% Nickel Steel for Ships and Performance Evaluation of the Welded Joint. *J. Weld. Join.* **2019**, *37*, 555–563. [[CrossRef](#)]
6. Yun, T.; Oh, W.; Lee, B.; Lee, C.; Na, H.; Choi, J.; Kim, I. A Study on Optimization of Fillet in Laser Welding Process for 9% Ni Steel Using Gradient-Based Optimization Algorithm. *J. Weld. Join.* **2020**, *38*, 485–492. [[CrossRef](#)]
7. Kim, J.; Kim, J.; Kang, S.; Chun, K. Laser Welding of ASTM A553-1 (9% Nickel Steel) (PART I: Penetration Shape by Bead on Plate). *Metals* **2020**, *10*, 484. [[CrossRef](#)]
8. Kim, J.; Kim, J. Laser Welding of ASTM A553-1 (9% Nickel Steel) (PART II: Comparison of Mechanical Properties with FCAW). *Metals* **2020**, *10*, 999. [[CrossRef](#)]
9. Huang, Z.; Cai, Y.; Mu, W.; Li, Y.; Hua, X. Effects of laser energy allocation on weld formation of 9%Ni steel made by narrow gap laser welding filled with nickel based alloy. *J. Laser Appl.* **2018**, *30*, 032013. [[CrossRef](#)]
10. Trinh, L.N.; Lee, D. Welding of Thin Tab and Battery Case for Lithium-ion Battery Cylindrical Cell Using Nanosecond Pulsed Fiber Laser. *J. Weld. Join.* **2020**, *38*, 389–394. [[CrossRef](#)]
11. Choi, K.; Lee, J.; Hong, J.; Chung, W. A Study on the Variation of Physical Properties of Line-heated for Type-B LNG Fuel Tank with 9% Nickel Steel Plate. *J. Korean Soc. Manuf. Process. Eng.* **2020**, *19*, 89–97. [[CrossRef](#)]
12. Park, J.; Kim, Y.; Baek, H.; Cho, S. A study on process development of super-TIG welding for 9% nickel steel with Alloy 625. *J. Manuf. Process.* **2019**, *40*, 140–148. [[CrossRef](#)]
13. Pyo, C. A Study for Heat Source Model for Fiber Laser Welding with Global Optimization Algorithm Part I. Verification of Multi Layered Heat Source Model. *J. Korean Soc. Mech. Technol.* **2021**, *23*, 137–144.
14. Pyo, C. A Study for Heat Source Model for Fiber Laser Welding with Global Optimization Algorithm Part II. Comparison of Optimization Algorithms. *J. Korean Soc. Mech. Technol.* **2021**, *23*, 226–233.
15. Pyo, C. A Study for Heat Source Model for Fiber Laser Welding with Global Optimization Algorithm Part III. Analysis of the parameters with welding power. *J. Korean Soc. Mech. Technol.* **2021**, *23*, 492–498.
16. Goldak, J.; Chakravarti, A.; Bibby, M. A new finite element model for welding heat sources. *MTB* **1984**, *15*, 299–305. [[CrossRef](#)]
17. Chujutalli, J.; Lourenço, M.; Estefen, S. Experimental-based methodology for the double ellipsoidal heat source parameters in welding simulations. *Mar. Syst. Ocean Technol.* **2020**, *15*, 110–123. [[CrossRef](#)]
18. Gao, Z.; Jiang, P.; Mi, G.; Cao, L.; Liu, W. Investigation on the weld bead profile transformation with the keyhole and molten pool dynamic behavior simulation in high power laser welding. *Int. J. Heat Mass Transf.* **2018**, *116*, 1304–1313. [[CrossRef](#)]
19. Dal, M.; Fabbro, R. [INVITED] An overview of the state of art in laser welding simulation. *Opt. Laser Technol.* **2016**, *78*, 2–14. [[CrossRef](#)]
20. Kim, J.; Jang, B.; Kim, Y.; Chun, K. A study on an efficient prediction of welding deformation for T-joint laser welding of sandwich panel PART I: Proposal of a heat source model. *Int. J. Naval Arch. Ocean* **2013**, *5*, 348–363. [[CrossRef](#)]
21. Farrokhi, F.; Endelt, B.; Kristansen, M. A numerical model for full and partial penetration hybrid laser welding of thick-section steels. *Opt. Laser Technol.* **2019**, *111*, 671–686. [[CrossRef](#)]
22. Xu, G.; Wu, C.; Qin, G.; Wang, X.; Lin, S. Adaptive volumetric heat source models for laser beam and laser + pulsed GMAW hybrid welding processes. *Int. J. Adv. Manuf. Technol.* **2011**, *57*, 245–255. [[CrossRef](#)]
23. Evdokimov, A.; Springer, K.; Doynov, N. Heat source model for laser beam welding of steel-aluminum lap joints. *Int. J. Adv. Manuf. Technol.* **2017**, *93*, 709–716. [[CrossRef](#)]
24. Kik, T. Heat Source Models in Numerical Simulations of Laser Welding. *Materials* **2020**, *13*, 2653. [[CrossRef](#)]
25. Kim, K.; Nam, K.; Lee, J.; Seo, J.; Cho, H. Finite element analysis for prediction of bead shape of Nd:YAG laser butt welding. *J. Korean Soc. Mar. Eng.* **2008**, *32*, 137–246.
26. Rahman, J.; Vasudevan, C.; Muthukumar, S.; Ravi, R.; Chandrasekhar, K. Simulation of laser butt welding of AISI 316L stainless steel sheet using various heat sources and experimental validation. *J. Mater. Process. Technol.* **2015**, *219*, 48–59. [[CrossRef](#)]
27. Rong, Y.; Mi, G.; Xu, J.; Huang, Y.; Wang, C. Laser penetration welding of ship steel EH36: A new heat source and application to predict residual stress considering martensite phase transformation. *Mar. Struct.* **2018**, *61*, 256–267. [[CrossRef](#)]
28. Unni, K.; Vasudevan, M. Determination of heat source model for simulating full penetration laser welding of 316 LN stainless steel by computational fluid dynamics. *Mater. Today Proc.* **2021**, *45*, 4465–4471. [[CrossRef](#)]
29. Artinov, A.; Bachmann, N.; Rethmeier, M. Equivalent heat source approach in a 3D transient heat transfer simulation of full-penetration high power laser beam welding of thick metal plates. *Int. J. Heat Mass Transf.* **2018**, *122*, 1003–1013. [[CrossRef](#)]
30. Agarwal, G.; Gao, H. Murugaiyan Amirthalingam, Marcel Hermans, Study of Solidification Cracking Susceptibility during Laser Welding in an Advanced High Strength Automotive Steel. *Metals* **2018**, *8*, 673. [[CrossRef](#)]
31. Yang, H. A Study on Heat Flow of Laser-Welded Dissimilar Steel Joints with Gap. *J. KIMST* **2007**, *10*, 5–15.
32. Lee, K.; Yun, G. A Finite Element Model of Melt Pool for the Evaluation of Selective Laser Melting Process Parameters. *J. KIMST* **2020**, *23*, 195–203. [[CrossRef](#)]
33. Ruolin, Z.; Xin, T.; Lidong, X.; Fenggui, L. Study of molten pool dynamics and porosity formation mechanism in full penetration fiber laser welding of Al-alloy. *Int. J. Heat Mass Transf.* **2020**, *148*, 119089.
34. Zhou, Q.; Wang, Y.; Choi, S.; Cao, L.; Gao, Z. Robust optimization for reducing welding-induced angular distortion in fiber laser keyhole welding under process parameter uncertainty. *Appl. Therm. Eng.* **2018**, *129*, 893–906. [[CrossRef](#)]
35. Ai, Y.; Jiang, P.; Shao, X.; Li, P.; Wang, C. A three-dimensional numerical simulation model for weld characteristics analysis in fiber laser keyhole welding. *Int. J. Heat Mass Transf.* **2017**, *108*, 614–626. [[CrossRef](#)]

36. Pyo, C.; Kim, J.; Kim, J. Estimation of Heat Source Model's Parameters for GMAW with Non-linear Global Optimization—Part I: Application of Multi-island Genetic Algorithm. *Metals* **2020**, *10*, 885. [[CrossRef](#)]
37. Deng, D. FEM prediction of welding residual stress and distortion in carbon steel considering phase transformation effects. *Mater. Des.* **2009**, *30*, 359–366. [[CrossRef](#)]
38. Deng, D.; Murakawa, H. Numerical simulation of temperature field and residual stress in multi-pass welds in stainless steel pipe and comparison with experimental measurements. *Comput. Mater. Sci.* **2006**, *37*, 269–277. [[CrossRef](#)]
39. Wang, W.; Mo, R.; Zhang, Y. Multi-Objective Aerodynamic Optimization Design Method of Compressor Rotor Based on Isight. *Procedia Eng.* **2011**, *15*, 3699–3703. [[CrossRef](#)]
40. Hahn, Y.; Cofer, J. Design Study of Dovetail Geometries of Turbine Blades Using Abaqus and Isight. In Proceedings of the ASME Turbo Expo 2012: Turbine Technical Conference and Exposition, Copenhagen, Denmark, 11–15 June 2012; Volume 7, pp. 11–20.
41. Park, M.; Kim, J.; Pyo, C.; Kim, J.; Chun, K. A Study on Determining Weld Joint Hardening and a Quality Evaluation Algorithm for 9% Nickel Weld Joints Using the Dilution Ratio of the Base Material in Fiber Laser Welding. *Metals* **2021**, *11*, 1308. [[CrossRef](#)]
42. Lee, H.; Kang, G. Calculation of Material Properties with JMatPro for the Process Simulation. In Proceedings of the Korean Society for Technology of Plasticity Conference, Chuncheon, Korea, 8 May 2008; pp. 142–145.
43. Casalino, G.; Contuzzi, N.; Minutolo, M.; Mortello, M. Finite element model for laser welding of titanium. *Procedia CIRP* **2015**, *33*, 434–439. [[CrossRef](#)]
44. D'Ostuni, S.; Leo, P.; Casalino, G. FEM Simulation of Dissimilar Aluminum Titanium Fiber Laser Welding Using 2D and 3D Gaussian Heat Sources. *Metals* **2017**, *7*, 307. [[CrossRef](#)]
45. Lin, J.; Zhong, Y.; Li, E.; Lin, X.; Zhang, H. Multi-agent simulated annealing algorithm with parallel adaptive multiple sampling for protein structure prediction in AB off-lattice model. *Appl. Soft Comput.* **2018**, *62*, 491–503. [[CrossRef](#)]
46. Saini, V.; Singla, S. Parameter Optimization of SAW in Hardfacing Process Using Hybrid Approach of Adaptive Stimulated Annealing and Neural Networks. *Asian J. Eng. Appl. Technol.* **2012**, *1*, 16–20.